Aerodynamics and wake flow characteristics of a four-cylinder cluster

Cung H. Nguyen[a], Saad Inam[b], Davide Lasagna[b], Zheng-Tong Xie[b,*]

[a] *School of Science, Engineering and Environment, University of Salford, UK*

[b] *Faculty of Engineering and Physical Sciences, University of Southampton, UK*

Abstract

The aerodynamic behaviour and wake flow of a cluster of two-dimensional sharp-edged bluff bodies exhibits extremely complex unsteady phenomena in both near and far fields. Due to the high cost of wind-tunnel experiments and numerical simulations, a complete understanding of wake flows and a description of their characteristics are lacking. This paper presents large-eddy simulations (LES) in different flow/wind directions for a cluster of 2×2 aligned square cylinders, at a separation distance in streamwise and cross-wind directions equal to cylinder side length, and at Reynolds number $Re = 22,000$ based on the single cylinder side length D. The case at 0° incidence shows an evident channel-type flow in the along-wind street/gap, and at its exit an irregularly pulsing jet with an intense shedding of large vortices. The wavelet analyses of the side force/lift coefficient and instantaneous velocities in the wake show that the characteristic length and time scales of the large vortical structures in the far-field wake are close to the cluster size $2D$; this is the so called 'cluster effect'. The cluster effect increases monotonically as the flow incidence angle increases. At a large incidence angle in the near-field wake, the cylinder-scale flow structures are much weaker compared to the cluster-scale structures. At the incidence angle of 45°, the overall wake flow and the aerodynamic characteristics are well scaled by the scale approximately equal to $2D$. Nevertheless, the interaction between cylinders significantly affects the aerodynamics performance of the individual cylinders. The drag and lift coefficients of the individual cylinders differ substantially from each other in the cluster, and are significantly different from observations on a single isolated cylinder too.

Keywords: LES, square cylinder, cylinder cluster, vortex shedding, wake characteristics, lift coefficient, wake interaction

*Corresponding author
Email address: Z.Xie@soton.ac.uk (Zheng-Tong Xie)

1. Introduction

1.1. Aerodynamic characteristics of a cluster of tall buildings and its wake flow

Many cities around the world are growing rapidly bigger and taller. More isolated and clustered tall buildings have been being built or are to be built. This change may significantly affects the urban environment, e.g. street-level winds, the dispersion of pollutants, heat fluxes and the temperature distribution. On the other hand, the changed wind environment affects the aerodynamic performance of the buildings, such as wind loading and indoor ventilation.

Studies on wake flows of a cluster of tall buildings require a domain greater than the neighbourhood scale ($\approx$ 1 km), and a Reynolds number greater than the critical one (Re $\approx 10^4$). The requirements of the large domain scale and the necessary building size challenge the available wind tunnel facilities, as well as the computational fluid dynamics approaches, despite the fast growing computing capability. Field experiments are able to provide full-scale data, e.g. at the Reynolds number $Re > 10^7$, and the Richardson number $Ri >> 1$, which are nevertheless expensive to obtain, and are usually scattered due to the varying meteorological conditions. Consequently, it remains challenging to understand and quantitatively describe the aerodynamic characteristics (e.g. force coefficients) of a cluster of buildings and its wake flow.

1.2. Aerodynamics of clusters of square cylinders

The wake flow of a cluster of two-dimensional (i.e. infinite in the spanwise/crosswind direction) square cylinders exhibits extremely complex phenomena in both the near and far fields, and lacks of good understanding and a quantitative description of its characteristics (e.g. Sau et al., 2007, Burattini and Agrawal, 2013, Agrawal et al., 2006, Han et al., 2014, Alam et al., 2011, 2002, Du et al., 2021, Kahil et al., 2019, Zhang et al., 2019). A very brief review is given below.

1.2.1. A pair of side-by-side square cylinders

A number of studies (Sau et al., 2007, Burattini and Agrawal, 2013, Agrawal et al., 2006) are reported in the literature on a pair of side-by-side cylinders in flows at Reynolds number around 100. Burattini and Agrawal (2013) studied wake interaction of two side-by-side square cylinders at a Reynolds number equal to 73, as a function of the spacing between cylinders. They noticed that the Strouhal number of vortex shedding was almost constant and near 0.16, within a range of spacing $0.5d$ to $6d$, where d is the cylinder side length. Han et al. (2014) studied the wake characteristics of two side-by-side square cylinders at a Reynolds number 22,000.

Alam et al. (2011) experimentally studied wake flow of two side-by-side square cylinders at a Reynolds number 47,000 at a centre-to-centre spacing pitch ratio ranging from P/D 1.02 to 6, where P is the centre-to-centre spacing. They identified four wake flow regions. First, the

single-body regime $\mathscr{A}$ was identified at $P/D < 1.3$, where the two cylinders were close enough to behave as a single body, forming a single staggered vortex street. The instantaneous velocity in the wake had a primary frequency which was approximately half of the shedding frequency of an isolated cylinder. Second, the two-frequency region $\mathscr{B}$ occurred at $P/D = 1.3 - 2.2$, where the gap flow between the cylinders was biased with adequate momentum to form one narrow and one wide street, which were respectively associated with a high and a low Strouhal number St. The former and latter were close to 0.5 and 1.5 times of the St of an isolated cylinder, respectively. Third, the transition region $\mathscr{C}$ was identified at $P/D = 2.2 - 3.0$, where the narrow and wide streets were still frequently observed as in the regime $\mathscr{B}$, while they switched from time to time to two anti-phased streets, because of the more energetic gap flow (compared to that in region $\mathscr{B}$) between the cylinders injecting into the wake and inducing the symmetry of wake. Consequently, three frequencies were identified from the power spectra of the wake velocities, i.e. 0.5, 1 and 1.5 times of the St of an isolated cylinder. Fourth and last, the coupled vortex shedding regime occurred at $P/D > 3.0$. At $P/D = 3.0 - 4.6$, the two vortices were shed predominantly in anti-phased pattern, due to the energetic gap flow between the cylinders, which was denoted sub-regime $\mathscr{D}1$. At $P/D > 4.6$, the two vortices were shed both in anti- and in-phase patterns, which was denoted sub-regime $\mathscr{D}2$. In regime $\mathscr{D}$, the primary frequency of the wake velocities was close to that of the single isolated cylinder.

1.2.2. Two square cylinders in a tandem

Alam et al. (2002) studied the aerodynamic interaction of two square prisms in a tandem arrangement with a variation of the centre-to-centre spacing ratio $1.5 < P/D < 12$, at $Re = 56,000$. The Strouhal number St calculated from the power spectrum of the fluctuating lift force acting on the downstream prism was within a very narrow range $0.10 < St < 0.13$. In particular, Alam et al. (2002) showed $St \approx 1.25$ at $P/D = 2$. Du et al. (2021) carried out wind tunnel experiments to study aerodynamic interaction of two square cylinders at $Re = 80,000$, a centre-to-center spacing ratio $P/D = 1.75$ and various incidence angles, in an aligned arrangement. The estimated Strouhal numbers of the lift coefficients of the two cylinders in the aligned arrangement were both greater than 0.1 for small incidence angles ($\alpha \leq 20°$). Both the data in Alam et al. (2002) and Du et al. (2021) may suggest that the two square cylinders in tandem do not evidently change the wake flow.

1.2.3. An array of 2-by-2 aligned square cylinders

It is worth noting that there are only a few studies for the 2-by-2 cylinders arrangement, mainly for low Reynolds numbers. Kahil et al. (2019) reported flows around four circular cylinders in square arrangement at a sub-critical Reynolds number 3000. They detected three distinct biased modes for a ratio of pitch to cylinder diameter ranging from 1.25 to 1.5, where the spacing was the gap width between two in-line cylinders. Mode 1 was defined when the wake of the entire cluster of cylinders drifted to one side within a certain period, while Mode 2 was defined for the reverse of flow topology of Model 1. Mode 3 was defined when the wake

had no preferred direction. The authors did not report the separation time of each mode due to the complexity of the physics.

Zhang et al. (2019) carried out water tunnel experiments to study the wake flow and aerodynamic forces of an array of 2-by-2 aligned square cylinders with a ratio of pitch to cylinder side size P/D ranging from 2 to 5, at incidence angles $\alpha = 0° - 45°$ and $Re = 8,000$. The performance of the unsteady lift and drag was extremely complicated in most of the configurations. Nevertheless, it was evident that the primary frequency of the lift coefficients of the downstream cylinders with $P/D = 2$ at $\alpha = 45°$ were $f = 1.23$ Hz, which are almost half of the primary frequency $f = 2.57$ Hz of the lift coefficients of the four cylinders with $P/D = 4$ at $\alpha = 0°$. Zhang et al. (2019) explained that this frequency, which was much lower than the vortex shedding frequency, corresponding to the quasi-steady, low frequency 'galloping and flutter' type of vibration commonly found in the case of rectangular and square cylinders. It is worth noting that the lower frequency $f = 1.23$ Hz measured in Zhang et al. (2019) corresponds to the Strouhal number $St = 0.062$, while the higher frequency $f = 2.57$ Hz corresponds to $St = 0.129$, which is very close to the primary vortex shedding frequency $St = 0.13$ of an isolated cylinder (see Table 3 and Bearman and Obasaju (1982a), Trias et al. (2015), Chen et al. (2020)). This suggested the strong cluster effect of four square cylinders at $\alpha = 45°$, which is a fluid-dynamic mechanism, but not a fluid-structure interaction phenomenon.

Du et al. (2021) also studied aerodynamic interaction of two square cylinders in an arrangement with aligned diagonals, at various incidence angles and a centre-to-center spacing ratio $P/D = 1.75$. It is highlighted that the narrowest tip-tip gap between the two cylinders was about $0.34D$. At $\alpha = 35°$, two evident dimensionless frequencies $St = 0.07$ and 0.21 of the fluctuating lift were observed. Note that the former and the latter were respectively 0.5 and 1.5 times of the shedding frequency of an isolated cylinder. At $\alpha = 70°$, two strong peaks in the spectrum of the fluctuating lift were observed at $St = 0.06$ and 0.27. For $0 < \alpha \leq 17.5°$, the dominant frequency was identified approximately at $St = 0.1$. Although it was complicated to draw a conclusive remark on the impact of wake flow, these results suggested that a cluster effect does occur at some incidence angles.

1.3. The current large-eddy simulation study

Up to the authors' knowledge, no study has been published on the correlation of the wake flow and the aerodynamic forces for a cluster of 2-by-2 cylinders, neither a conclusive remark of the scaling of the dominant vortex shedding frequency has been drawn consistently from the two sets of data. The present large-eddy simulation(LES) study (e.g. Section 3) of aerodynamic forces and wake flow is focused on the dominant dimensionless vortex shedding frequency (i.e. the Strouhal number St) to bridge the knowledge gap of the connection between the aerodynamic forces of the cluster and the wake flow. It aims to shed some light on the mechanism of

flow around a cluster of cylinders and to provide an implication for relevant applications, such as the design of a cluster of tall buildings in cities.

This paper presents large-eddy simulations at a moderately large Reynolds number ($Re = 22,000$) for single and 2-by-2 square prism arrangements, which are homogeneous in the spanwise direction. Different flow incidence angles were considered. The paper is organised as follows. The computational methods including LES and wavelet analysis are introduced in Sections 2.1-2.2. The numerical setup is introduced in Section 2.3. The validation and sensitivity tests are presented in Section 2.4. Section 3 and 4 show the characteristics of wake flow and aerodynamic forces, respectively. Conclusions and discussions are presented in Section 5.

2. Computational methods, numerical settings, and validations

2.1. Large Eddy Simulations

Large Eddy Simulations (LES) embedded in the open source code OpenFOAM-v2006 was performed to solve the filtered, incompressible Navier-Stokes equations,

$$\frac{\partial \bar{u}_i}{\partial x_i} = 0, \tag{1}$$

$$\frac{\partial \bar{u}_i}{\partial t} + \frac{\partial}{\partial x_j}(\bar{u}_i \bar{u}_j) = -\frac{\partial \bar{p}}{\rho \partial x_i} + \frac{\partial}{\partial x_j}\left(\nu \frac{\partial \bar{u}_i}{\partial x_j}\right) + \frac{\partial \tau_{ij}}{\partial x_j}, \tag{2}$$

where $\bar{u}_i$ and $\bar{p}$ are the filtered velocity and pressure, respectively; ρ is the density; ν is the kinematic viscosity. The kinematic sub-grid scale (SGS) stresses τ_{ij} are modelled using the Boussinesq assumption,

$$\tau_{ij} = \bar{u}_i \bar{u}_j - \overline{u_i u_j} = 2\nu_t \bar{S}_{ij} - \frac{1}{3}\delta_{ij}\tau_{kk}, \tag{3}$$

in which δ_{ij}, ν_t, and $\bar{S}_{ij}$ are the delta Kronecker, the kinematic SGS viscosity and the rate-of-strain tensor for the resolved scales, respectively. Both the Smagorinsky and the mixed time-scale (Inagaki et al., 2005) SGS models were tested in the study, and no visible discrepancy was identified.

2.2. Wavelet analysis

The vortex shedding, wake flow and aerodynamic forces of a cluster of square cylinders display multi-scale behaviour (e.g. Kahil et al., 2019, Zhang et al., 2019). The conventional Fourier analysis is used to process a sufficiently long time series of a stationary process, but can struggle to identify energetic and localised events in short time series. The windowed Fourier analysis splits the time series into a number of short fixed-length segments, and then applies the Fourier transform separately on each segment (Perrier et al., 1995). The pre-defined fixed resolution (i.e. the segment length) constrains the application of the windowed Fourier analysis. In contrast to Fourier transform approaches, the wavelet analysis has the inherent ability to capture local-time spectra of a non-stationary signal (Mahrt, 1991, Perrier et al., 1995,

Horiguchi et al., 2012, Nguyen et al., 2022), and can be used for identifying multiple scales in wake flows and in the time series of aerodynamic forces.

We noticed that the wake flow and the aerodynamic forces were non-stationary, and decided to use wavelet analysis in this study. Below is a brief of wavelet analysis. The wavelet transformation of a time series signal $\xi(\tau)$ (e.g. a time series of the wake velocity or the aerodynamic force acting on an individual cylinder) is defined as follows

$$T_p(a,t) = \frac{1}{\sqrt{a}} \int_{-\infty}^{\infty} \Psi^* \left(\frac{\tau - t}{a} \right) \xi(\tau) \mathrm{d}\tau, \tag{4}$$

where T_p is the wavelet coefficient (scalogram), Ψ is the mother wavelet with the asterisk denoting the complex conjugate of the function, and a and t are respectively the scale and translation parameters. In this paper, the Morse wavelet function (Olhede and Walden, 2002) is employed.

For a clear identification of the energetic scales, the mean wavelet magnitude is used

$$\bar{S}(\tilde{n}) = \int_{-\infty}^{\infty} \left| T_p(\tilde{n}, t) \right| \mathrm{d}t, \tag{5}$$

where $\tilde{n} = fD/U_\infty$ is dimensionless frequency, being $f = 1/(2a)$ and U_∞ the frequency and the freestream velocity at inlet. For vortex shedding frequency, $\tilde{n}$ is commonly referred to as Strouhal number St.

The time-average wavelet magnitude $\bar{S}(\tilde{n})$ is calculated from the integration over the entire time duration of the wavelet coefficient. It provides an easier tool to identify the representative scales compared to the time-frequency scalogram map (see Figure 4 as an example).

2.3. Numerical setup

Two arrangements of square cylinders were considered: **Case 1**, with an isolated square cylinder of size D and infinite spanwise length, and **Case 2**, with a two by two array of square cylinders with the same dimension as in Case 1 and with a centre-centre spacing of $2D$ (see Fig. 1). The Reynolds number was $Re = 22,000$ based on the freestream speed U_∞ and the cylinder size D. Five flow incidence angles, $\alpha = 0°, 11.25°, 22.5°, 33.75°$ and $45°$ were simulated for Case 2. Figure 1a-b show the computational domain dimensions and the partition of the structured mesh for Case 1 ($27D \times 20D \times 4D$) and Case 2 ($56D \times 43D \times 4D$), respectively.

For Case 1, the structured mesh was chosen based on the settings as in the stationary square cylinder case in Chen et al. (2020). Moreover, for the purpose of sensitivity analysis, three resolutions were tested, including coarse mesh with 14 millions cells, medium mesh with 20 millions cells and fine mesh with 24 millions cells. The resolution of the first near wall grid was always equal to $D/200$, equivalent to less than 5 wall units. Other mesh parameters were the same as those of the stationary case in Chen et al. (2020). For Case 2, the mesh structure for

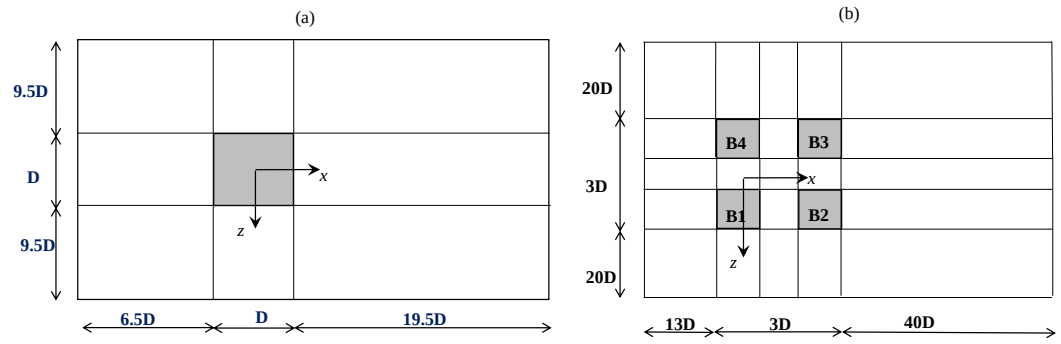

Figure 1: A sketch of the computational domain (not to scale) and its partition for structured mesh: (a) an isolated cylinder; (b) a cluster of 4 cylinders. The resolution in the near the single cylinder and the cluster region is 200 grid points per cylinder side D, giving the first grid resolution in wall unit less than 5.

all considered flow directions was based on that of Case 1 with the fine mesh cells, with a fine mesh of 73 million cells and the same near-wall resolution as Case 1.

Uniform velocities were imposed at the inlet (left) and top boundaries (Figure 1). Outflow boundary condition was imposed at the bottom and outlet (right) boundaries. In the spanwise direction, periodic boundary conditions were used. No-slip boundary condition was applied on the cylinder surfaces. For all simulated cases, the initial duration for LES was more than 150 t^*, the duration for average was more 200 t^*, where $t^* = tU_\infty/D$ is the non-dimensional time.

2.4. Validation of a single square cylinder and mesh sensitivity tests

Validation simulations for Case 1 were carried out at zero incidence angle and were compared to the LES data in Chen et al. (2020) obtained from an in-house code, the experimental data in Bearman and Obasaju (1982a), and the DNS data in Trias et al. (2015). Table 1 shows the time-averaged drag coefficient ($\bar{C}_D$), the root-mean-square ($r.m.s.$) value of the fluctuating lift coefficient ($\tilde{C}_L$) and the Strouhal number (St). The coefficients are hereafter normalised by the freestream speed U_∞ and the cylinder size D. The present LES data with the "fine mesh" agree well with the reference LES data (Chen et al., 2020), as the crucial numerical settings are identical. All the data-sets including the present ones show an identical Strouhal number $St = 0.13$. This may suggests that the Strouhal number is less sensitive than the other quantities, e.g. $\tilde{C}_L$. The present LES slightly under-predicts $\tilde{C}_L$ compared to the DNS data, whereas over-predicts it compared to the experimental data. This is likely because $\tilde{C}_L$ is sensitive to numerical and experimental conditions, e.g. time and spatial resolutions. As the fine mesh provided results in agreement with data in the literature (e.g. Chen et al., 2020), it was used as the base mesh for the cluster of four cylinders.

To ensure the accuracy at oblique inflows while the structured mesh was unchanged for different flow indecencies, a further mesh sensitivity test was carried out. The mesh was further

refined from the "fine mesh", and the total number of cells reached to 158.5 million. This "finer mesh" was used for testing flow around the cluster at $\alpha = 45°$. Table 2 shows mean and *r.m.s.* drag ($\bar{C}_{Di}$ and $\tilde{C}_{Di}$, respectively) and mean lift and *r.m.s.* lift ($\bar{C}_{Li}$ and $\tilde{C}_{Li}$, respectively) coefficients of individual cylinders of the cluster. Overall the mean aerodynamic coefficients and *r.m.s.* data obtained from two mesh cases are in good agreement. A discrepancy of mean coefficients was visible, which was because the average duration was not sufficient enough to get fully converged mean and *r.m.s.* data for such highly non-stationary flows at $\alpha = 45°$ (see Figure 11). Nevertheless, this small uncertainty would not change the conclusive remarks made in the paper.

Table 1: Validation for the single cylinder at $Re = 22,000$ and $\alpha = 0°$

	Present (coarse mesh)	Present (medium mesh)	Present (fine mesh)	Chen et al. (2020)	Bearman and Obasaju (1982b)	Trias et al. (2015)
$\bar{C}_D$	2.06	2.01	2.22	2.25	2.1	2.18
$\tilde{C}_L$	1.17	1.11	1.41	1.45	1.2	1.71
St	0.13	0.13	0.13	0.13	0.13	0.13

Table 2: Mean and r.m.s drag ($\bar{C}_{Di}$ and $\tilde{C}_{Di}$, respectively) and mean lift and r.m.s lift ($\bar{C}_{Li}$ and $\tilde{C}_{Li}$, respectively) coefficients of individual cylinders of the cluster at $Re = 22,000$ and $\alpha = 45°$ for two meshes. The subscript 'i' denotes the cylinder identification number detailed in Figure 1

	$\bar{C}_{D1}$	$\bar{C}_{D2}$	$\bar{C}_{D3}$	$\bar{C}_{D4}$	$\bar{C}_{L1}$	$\bar{C}_{L2}$	$\bar{C}_{L3}$	$\bar{C}_{L4}$
Fine mesh	2.4	1.37	2.34	1.91	-0.4	0.02	0.36	-0.04
Finer mesh	2.16	1.33	2.15	1.75	-0.32	-0.02	0.3	-0.02
	$\tilde{C}_{D1}$	$\tilde{C}_{D2}$	$\tilde{C}_{D3}$	$\tilde{C}_{D4}$	$\tilde{C}_{L1}$	$\tilde{C}_{L2}$	$\tilde{C}_{L3}$	$\tilde{C}_{L4}$
Fine mesh	0.37	0.17	0.36	0.03	0.17	1.01	0.17	0.1
Finer mesh	0.34	0.16	0.34	0.03	0.14	0.95	0.14	0.07

3. Characteristics of lift coefficient of the cluster and the wake flow

The fine mesh (Table 2) was used for all the large-eddy simulations reported in the following sections and 8). Again, in the current study we focus more prominently in the region of the wake for $x/D \geq 3.0$, given the extreme complexity of the flow field between the cylinders and in the very near wake (e.g. $x/D < 3.0$), where the recirculation and the peak TKE can be identified (e.g. Knisely, 1990, Mueller, 2012, Cao and Tamura, 2016, Chen et al., 2020). In total, we placed ten probes in the wake region (Table 3) to record velocity time series. The spectral characteristics of recorded velocity fluctuations are analysed in the following sections, to elucidate the dynamics of the vortices shed past the cluster.

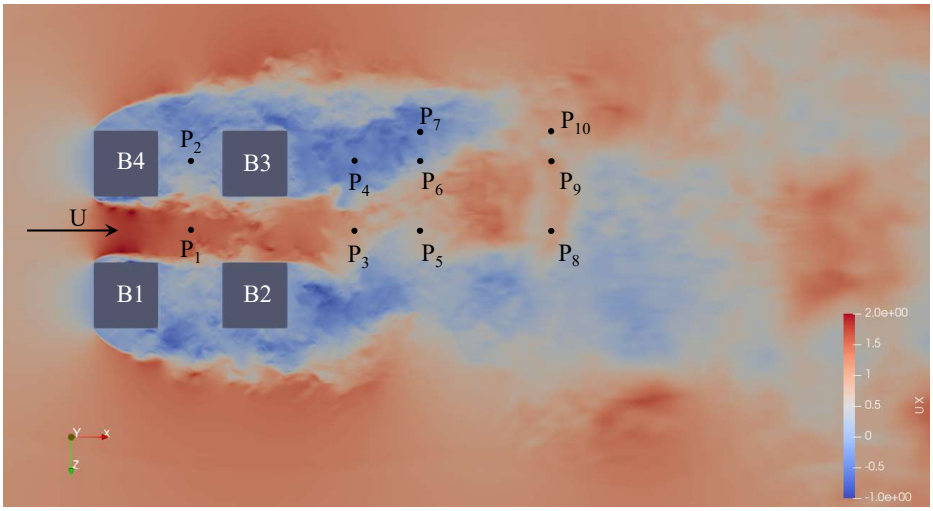

Figure 2: Example instantaneous velocity field u_x at $\alpha = 0°$ and locations of velocity probes

Table 3: Locations of the velocity probes placed in the wake region. See Fig. 1 for the reference system utilised

ID	P_1	P_2	P_3	P_4	P_5	P_6	P_7	P_8	P_9	P_{10}
x/D	1	1	3.5	3.5	4.5	4.5	4.5	6.5	6.5	6.5
z/D	0	-1	0	1	0	-1	-1.5	0	-1	-1.5

3.1. Case at $\alpha = 0°$

Figure 2 shows a snapshot of the instantaneous velocity u_x for the case $\alpha = 0°$. A strong channelling effect is observed in the along-wind spacing, with separation and reattachment on the inward sides of the front cylinders B1 and B4. This differs from observations around a single isolated square cylinder where flow reattachment does not occur (e.g. Chen et al., 2020). At the exit of the along-wind spacing, a pulsing jet flow is evident with intense vortices shed in a slightly asymmetric pattern. This shedding is slow and irregular,and is shown from the following analysis of the aerodynamic force coefficients and the wake velocity field.

Figure 3a shows the time-frequency scalogram map of the lift force coefficient C_L of cylinder B3 at $\alpha = 0°$ (left), and its time-averaged wavelet magnitude $\bar{S}(\tilde{n})$ (right). The force spectrum shows a dominant frequency $\tilde{n} = 0.14$, which is close to that of an isolated cylinder. It is worth noting that the lift force coefficient of the upstream cylinder B4 does not show any dominant frequency (not shown). In addition, the lift force coefficients of the cylinders B3 and B4 both show a weak peak at $\tilde{n} = 0.062$, which is approximately half of that of an isolated cylinder, suggesting a cluster effect.

Figure 3b shows the same as Figure 3a but for the summation of the lift force coefficients of the four cylinders. The total lift of the four cylinders show more complex spectrum than that for the cylinder B3. Different from the case of individual cylinder shown in Figure 3a, no dominant frequency is clearly shown. Instead, large wavelet magnitude occurs within a wide range of

frequency (e.g. $0.08 \leq \tilde{n} \leq 0.22$) with a peak at $\tilde{n} = 0.162$. The broadband spectrum suggests that multiple-scale vortices act on the cluster, of which the small ones are due to the unsteady channel flow between the cylinders, the pulsing jet at the exit between cylinders B2 and B3, and broken-down vortices from the large ones due to the jet. These structures are associated with the fluctuations of lift force on the individual cylinders.

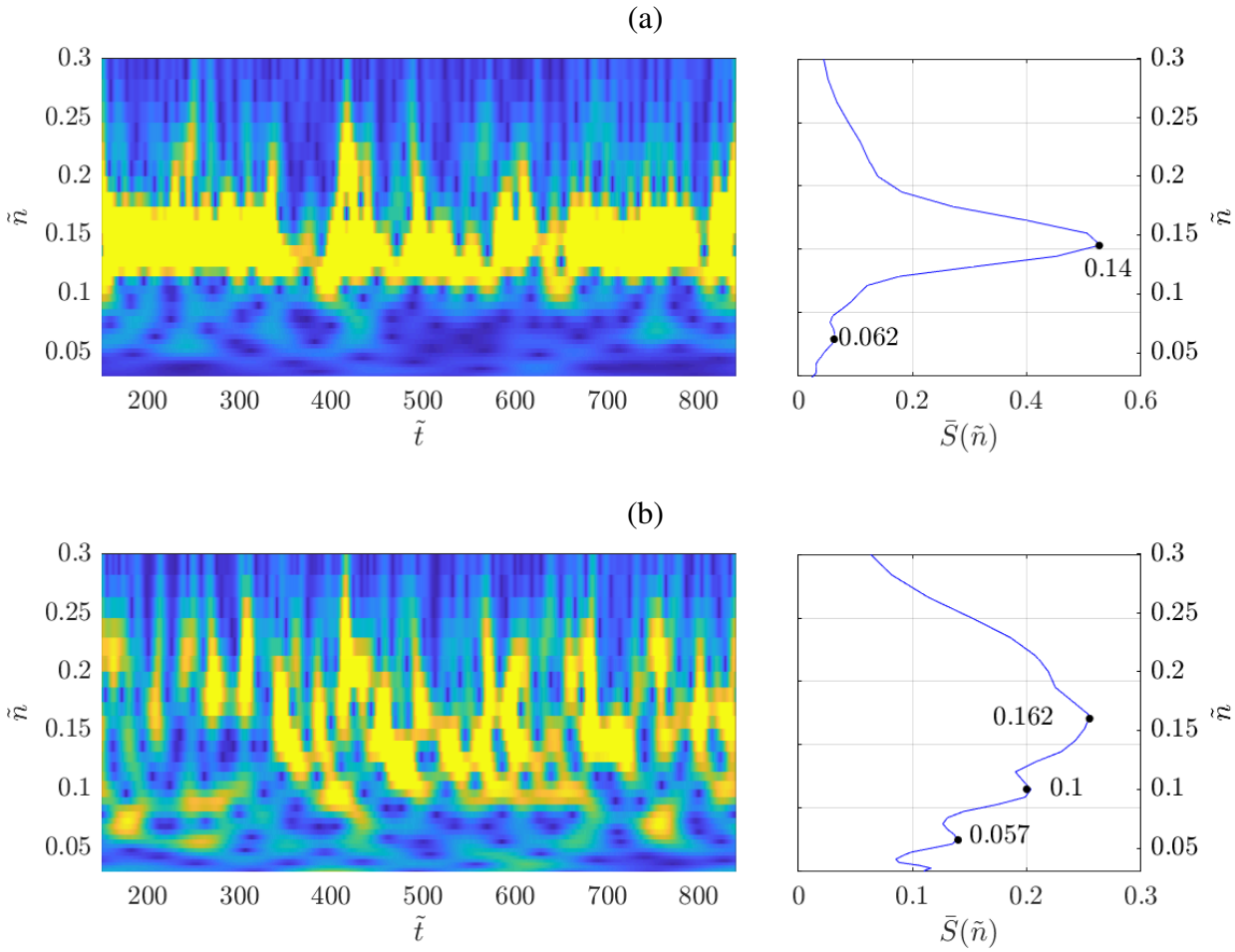

Figure 3: Time-frequency scalogram map (left) and the time-averaged wavelet magnitude(right) of (a) the lift force coefficient C_L of cylinder B3 and (b) summation of the lift force coefficients of the four cylinders at $\alpha = 0°$

Velocity time series sampled in the wake were also used to understand the characteristics of the vortices. Figure 4 shows the time-frequency scalogram map of the fluctuating streamwise velocity component at $\alpha = 0°$ (left) and the time-averaged wavelet magnitude $\bar{S}(\tilde{n})$ (right) at various locations in the wake. The data at the near-cluster probes P4 and P5 show a dominant frequency $\tilde{n} = 0.14$, which is the same as that of the lift of the downstream cylinder B3 and B2, and is slightly greater than that $\tilde{n}$ (i.e. St) $= 0.13$ of an isolated cylinder. This confirms as in Figure 3 that the vortex shedding frequency and the resultant frequency of lift force of the downstream cylinders are $\tilde{n} = 0.14$. Figure 4 shows clear secondary frequencies, which are close to the half of the dominant frequency $\tilde{n} = 0.14$. This is consistent to the secondary (lower) frequencies in the wavelet magnitude of lift coefficient in Figure 3. At probe P_{10}, which is the farthest one to the cluster, only the lower frequency $\tilde{n} = 0.062$ is visible. One might speculate

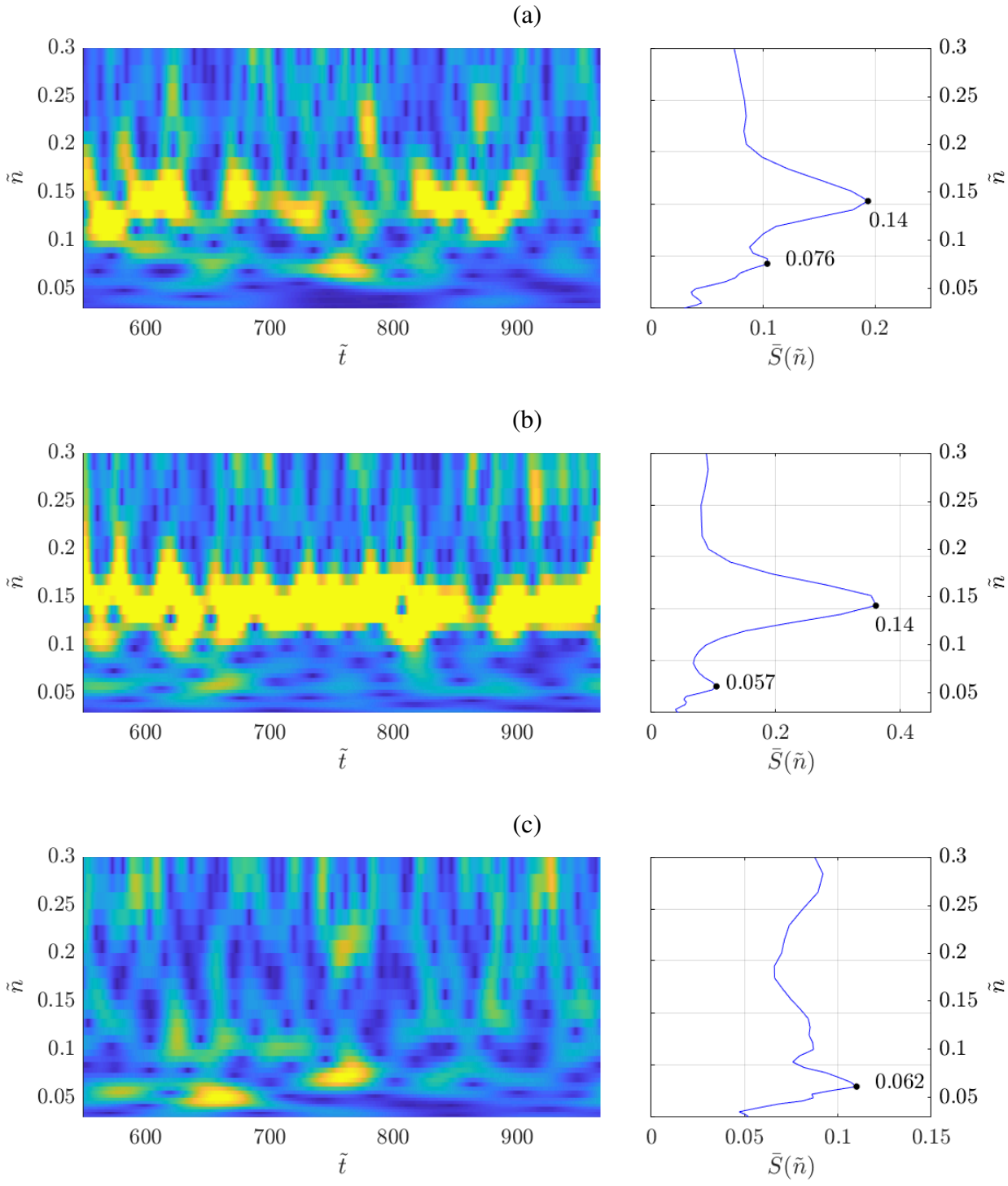

Figure 4: Time-frequency scalogram map (left) and the time-averaged wavelet magnitude(right) of the streamwise fluctuating velocity at $\alpha = 0°$ at locations (a) P_4; (b) P_5; (c) P_{10}

that the near-cluster vortices at $\tilde{n} = 0.14$ interact with the slow jet from the along-wind spacing, convert downstream and merge into larger vortices (see Figure 2).

The flow structure at $\alpha = 0°$ is the most complex one compared to the oblique inflow cases, in terms of the identification of the primary frequency of the vortex shedding. Given the extreme complexity of the lift coefficient signal of the individual cylinders, the following sections are focused on the total lift coefficient and the velocity time series sampled from several probes in the wake.

3.2. *Case at* $\alpha = 11.25°$

At $\alpha = 11.25°$, the vortex shedding pattern and the primary vortex shedding frequency were studied as for $\alpha = 0°$. As an illustrative example, Figure 5a shows the time-frequency scalogram map (left) and the time-averaged wavelet magnitude $\bar{S}(\tilde{n})$ (right) of the total lift coefficient C_L of the cluster. Figure 5b shows the same as Figure 5a, but for the streamwise velocity at probe P_5.

For isolated square cylinders, it is known (e.g Knisely, 1990, Norberg, 1993, Tamura and Miyagi, 1999, Mueller, 2012, Nguyen et al., 2020) that $\bar{C}_L$ and Strouhal number St (i.e. $\tilde{n}$) reach their peak values at a critical angle of incidence between $\alpha = 12° - 14°$. The dominant frequency $\tilde{n} = 0.076$ shown in Figure 5 is very close to half of the peak frequency ($\tilde{n} = 0.14 - 0.155$) of an isolated cylinder at the critical angle of incidence (e.g Tamura and Miyagi, 1999, Mueller, 2012). This confirms again the strong cluster effect of the flows between the four cylinders, resulting in a dominant vortex shedding frequency $\tilde{n} = 0.076$. This also suggests that the cluster behaves, as if it was an isolated, solid square cylinder with a width $2D$, in terms of the dominant shedding frequency.

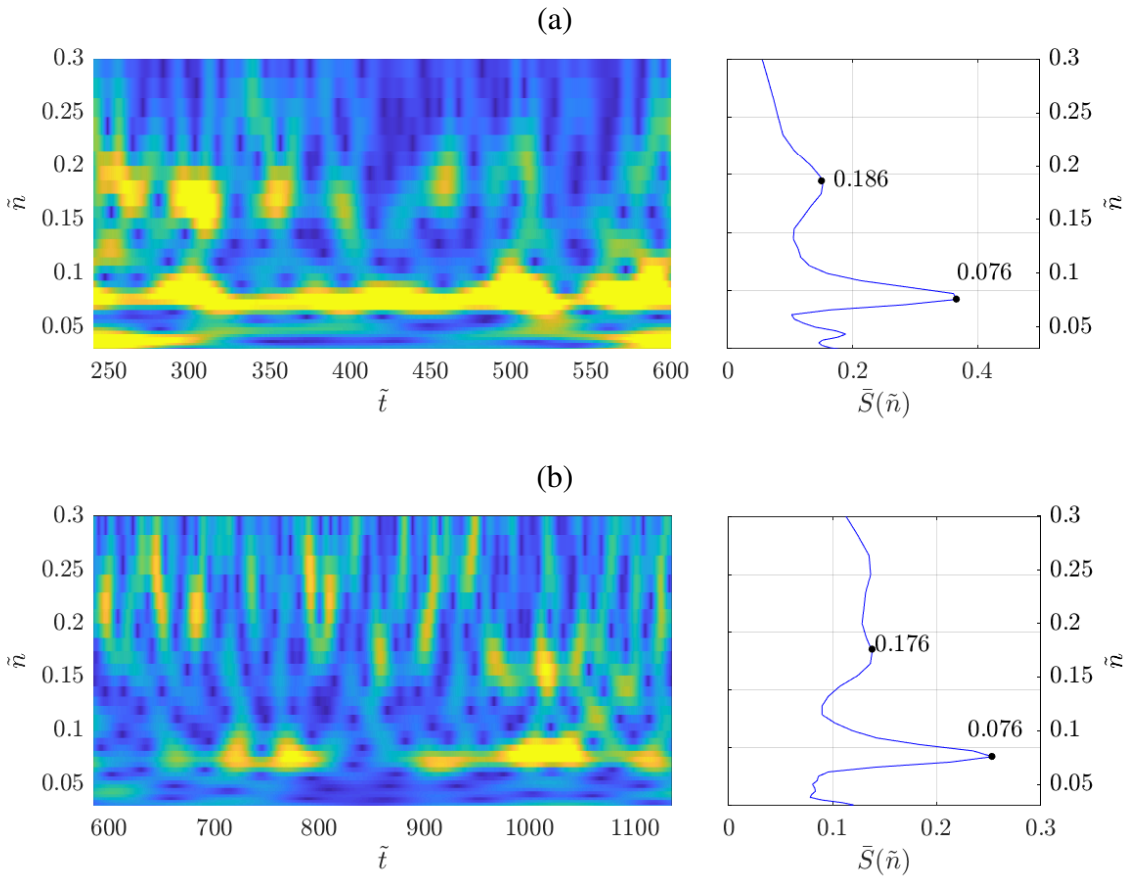

Figure 5: Time-frequency scalogram map (left) and the time-averaged wavelet magnitude (right) of (a) the sum of lift force coefficients of the four cylinders and (b) the streamwise fluctuating velocity at location P_5 at $\alpha = 11.25°$

3.3. *Case at* $\alpha = 22.5°$

Figure 6a shows the time-frequency scalogram map (left) and the time-averaged wavelet magnitude (right) of the total lift coefficient of the cluster at $\alpha = 22.5°$. Figure 6b shows the same as Figure 6a but for the streamwise fluctuating velocity at probe P_{10}. Similar to those at $\alpha = 11.25°$, the data in Figure 6 collectively shows a dominant frequency $\tilde{n} = 0.062$, which is very close to half of the dominant frequency $\tilde{n} \approx 0.127$ of an isolated square cylinder at $Re = 46,000$ and $\alpha = 20°$ (e.g. Mueller, 2012). Again, this suggests that the cluster behaves as a 2D-width solid square cylinder at $\alpha = 22.5°$.

The second harmonic frequency $\tilde{n} = 0.123$ is visible from the two wavelet spectra in Figure 6. This falls into the range of the dominant vortex shedding frequency $0.123 \leq \tilde{n}$ (i.e. St) ≤ 0.131 of of an individual isolated cylinder (e.g. Mueller, 2012), suggesting that the cylinder scale vortex plays an negligible role on the lift force and the velocities in wake region downstream $x = 6.5D$ from the cluster centre.

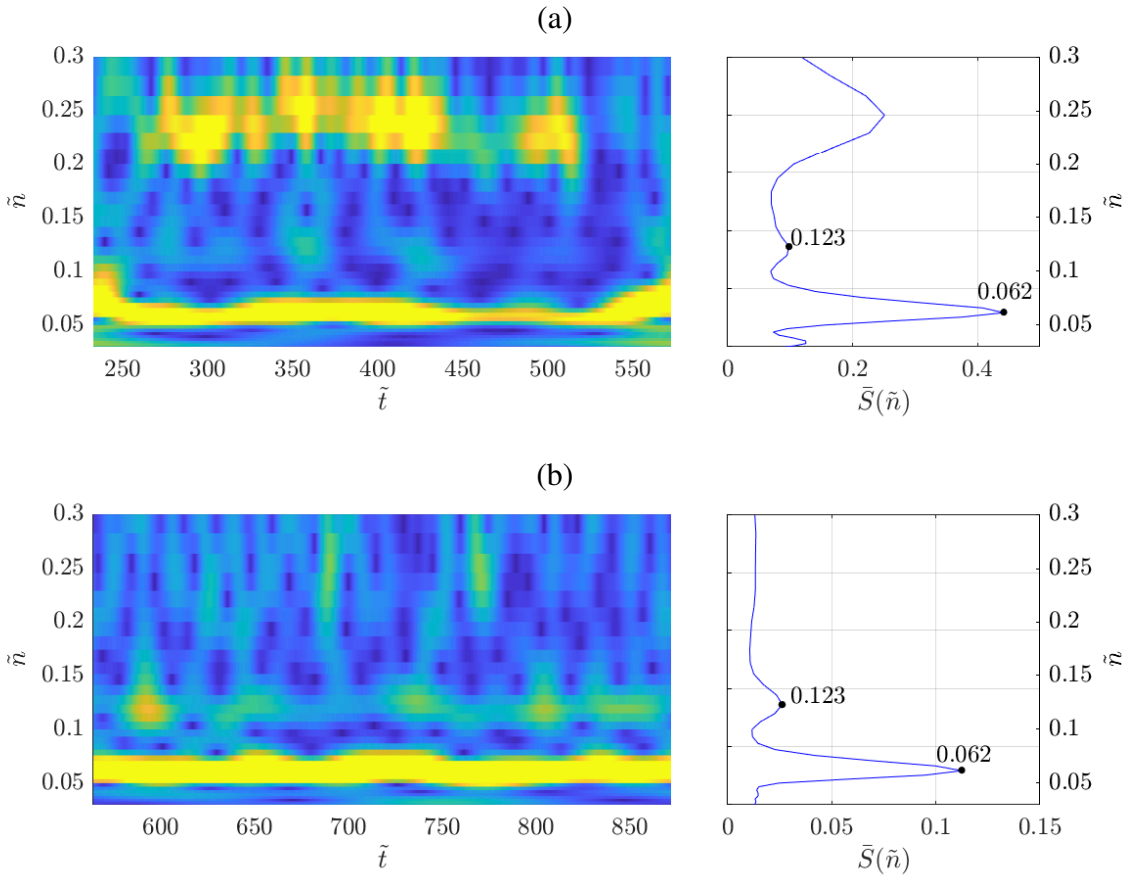

Figure 6: Time-frequency scalogram map (left) and the time-averaged wavelet magnitude (right) of (a) the sum of lift force coefficients of the four cylinders and (b) the streamwise fluctuating velocity at location P_{10} at $\alpha = 22.5°$

3.4. Case at $\alpha = 33.75°$

Figure 7 shows the same as Figure 6 but at $\alpha = 33.75°$. The data in Figure 7a and b collectively show a dominant frequency $\tilde{n} = 0.054$, equal to half of the secondary frequency $\tilde{n} = 0.107$. The latter is almost the same as that of an isolated square cylinder at $\alpha = 33°$ and $Re = 46,000$ (Mueller, 2012). This is consistent with those at $\alpha = 22.5°$ that the incoming flow 'sees' a more densely packed cluster than at $\alpha = 0,$ and $11.25°$, and the dominant vortex shedding frequency is more pronounced.

The second harmonic frequency, $\tilde{n} = 0.107$, is weakly visible from Figure 7a for the lift force data but more visible from Figure 7b for the fluctuating velocity in the wake. We noticed that the secondary shedding frequency is more evident at the probes closer to the cluster (not shown here). This is perhaps not surprising as the individual cylinders have more impact on the vortices shed at this scale.

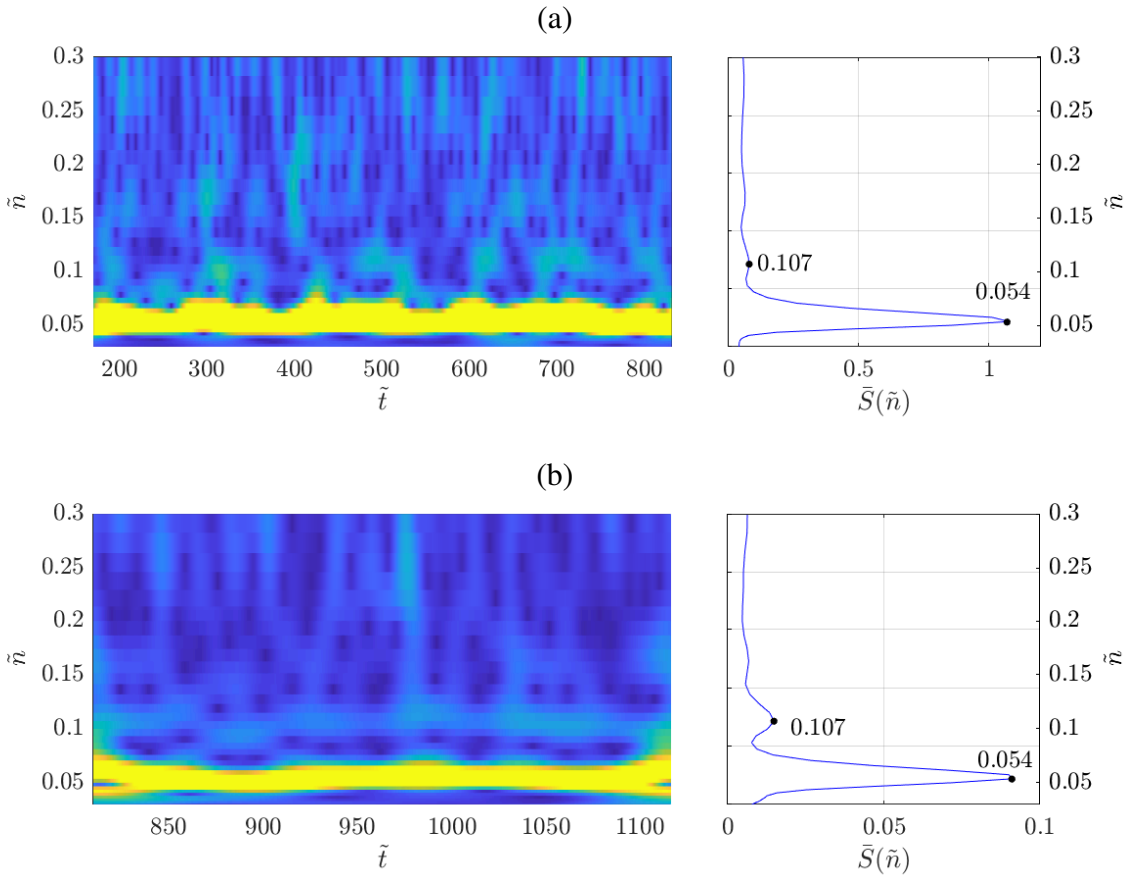

Figure 7: Time-frequency scalogram map (left) and the time-averaged wavelet magnitude (right) of (a) the sum of lift force coefficients of the four cylinders and (b) the streamwise fluctuating velocity at location P_{10} at $\alpha = 33.75°$

3.5. *Case at* $\alpha = 45°$

Figure 8 shows that the overall flow at $\alpha = 45°$ is asymmetric to the central plane along the flow direction, similar as the flow around a single isolated square cylinder. Separated flows at the sharp corners of cylinders B1, B3 and B4 are evident, while the separation around B4 is largely constrained by B1 and B3, resulting in nearly steady lift and drag, as discussed later in Figure 11. Cylinder B2 is entirely in the wake of three upstream cylinders, and is significantly impacted by the oscillatory wakes, as discussed later in Figure 11.

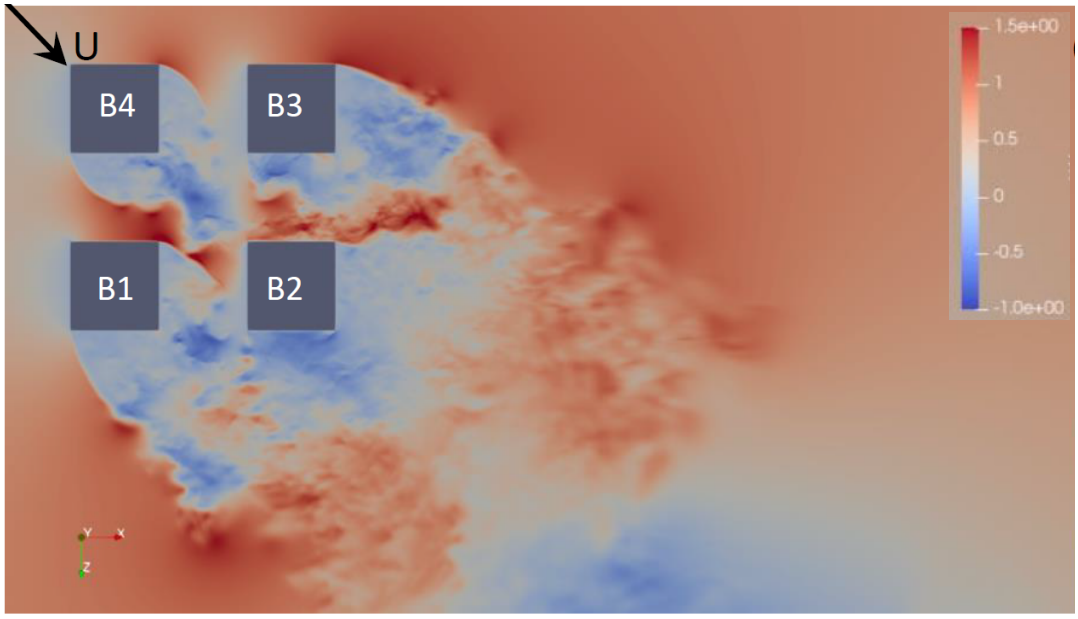

Figure 8: Instantaneous velocity field u_x at $\alpha = 45°$

Figure 9a shows the time-frequency scalogram maps (left) and the time-averaged wavelet magnitude (right) of the total lift coefficient of the cluster at $\alpha = 45°$. Figure 9b shows the same as Figure 9a but for the fluctuating velocity at location P_{10}. The data in Figure 9 collectively shows a dominant frequency of approximately $\tilde{n} = 0.05$, which is very close to half of the dominant frequency $\tilde{n} = 0.106$ for an isolated cylinder (Mueller, 2012). This again confirms that the cluster at $\alpha = 45°$ behaves as if it was an individual isolated cylinder with width equal to 2D. The higher harmonic frequency are hard to discern at $\alpha = 45°$ compared to the other incidence angles. It is worth noting that, at $\alpha = 45°$, the front area covered by the cylinders is equal to the maximum cross-section of the entire cluster including the spacing between the cylinders, which is aerodynamically the 'densest' configuration in all flow directions, and behaves the most like a single larger square cylinder with a width approximately equal to $2D$.

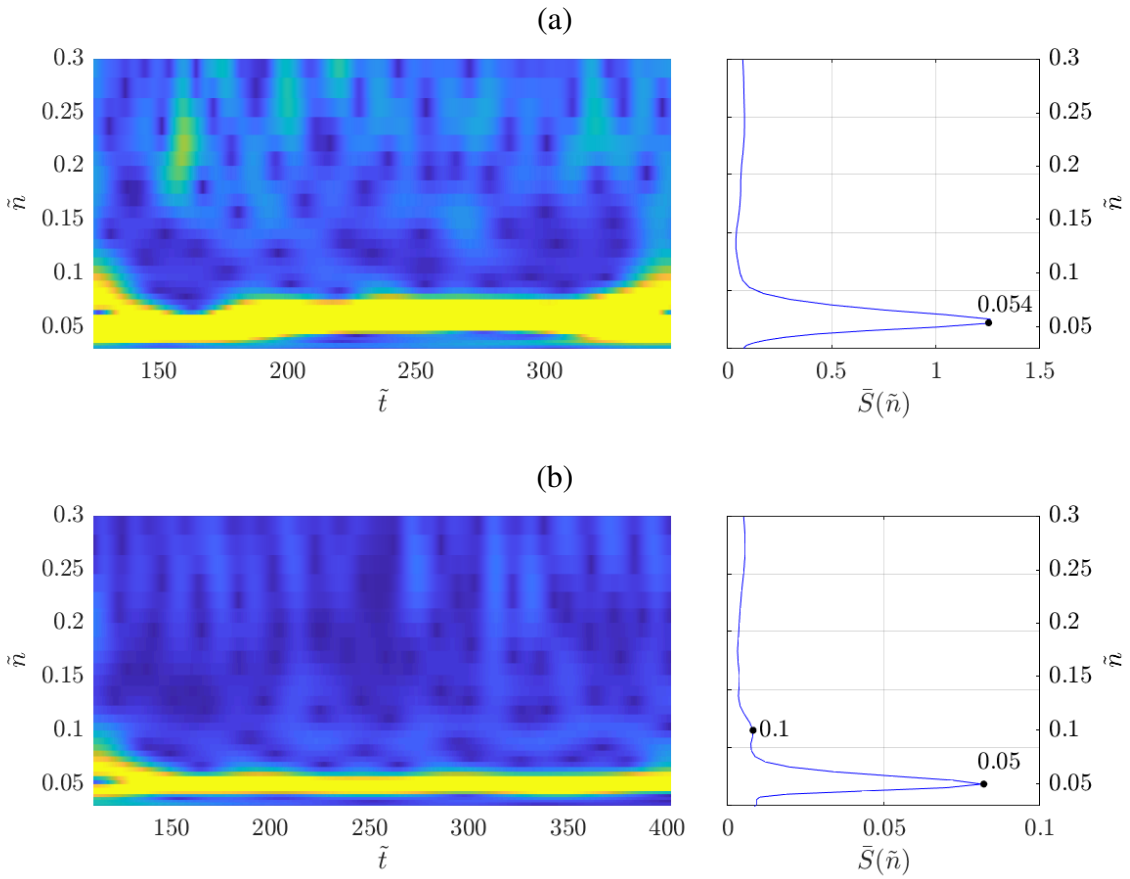

Figure 9: Time-frequency scalogram map (left) and the time-averaged wavelet magnitude (right) of (a) the sum of lift force coefficients of the four cylinders and (b) the streamwise fluctuating velocity at location P_{10} at $\alpha = 45°$

3.6. Summary and discussion

Overall, the dominant frequency of the lift force of the cluster of four square cylinders in oblique winds (i.e. $\alpha \neq 0°$) is identical as the dominant frequency of the sampled velocities at probes $x/D > 3.0$ downstream from the cluster. These collectively suggest not only that the whole cluster behaves as a single larger square cylinder with a width approximately $2D$, and also that the total lift force and the vortex shedding are well correlated. This is unexpected, as one might speculate that the size of the cluster including the spacing is $3D$. We argue that the separation between the cylinders, i.e. the 'permeability' of the cluster to the incoming flow, determines a change in the dynamics in both the near- and far-wake regions of the cluster, resulting in unsteady flow features whose time scale is well described $2D$.

At $\alpha = 0°$, the two downstream cylinders show a dominant vortex shedding frequency $\tilde{n} = 0.14$, which is slightly greater than that of a single isolated square cylinder, whereas the two upstream two cylinders and the entire cluster do not exhibit any prominent temporal behaviour, demonstrating higher complexity of flow characteristics compared to the oblique-wind case. Nevertheless, at the farthest downstream probe location (e.g. P_{10}) the wavelet variance spectrum showed a dominant frequency $\tilde{n} = 0.062$, which was nearly half of that of an isolated cylinder, corroborating the observation that the temporal dynamics of vortical structures in the far field can be scaled by $2D$.

Table 4 shows the dominant frequencies of the cluster and an isolated cylinder in Knisely (1990) and Mueller (2012). For the cluster, the $\tilde{n}(C_L, clus.)$ data are identical to $\tilde{n}(u_x, clus.)$ in oblique winds ($\alpha \neq 0°$), while at $\alpha = 0°$, $\tilde{n}(C_L, clus.)$ differs slightly from $\tilde{n}(u_x, clus.)$ due to the complex wake flow, e.g. the pulsing jet flow from the aloing-flow spacing. The data of $\tilde{n}(C_L, sing.)/\tilde{n}(C_L, clus.)$ at $0° \leq \alpha \leq 45°$ are approximately 2, suggesting that the dominant vortex shedding frequencies of the cluster scaled by $2D$, are approximately equal to the corresponding dominant frequency of an isolated single cylinder scaled by D.

Table 4: Dominant frequencies of the cluster and an isolated cylinder and the respective ratio. $\tilde{n}(C_L, clus.)$ and $\tilde{n}(u_x, clus.)$ are the dominant dimensionless frequencies of the cluster, calculated from C_L and u_x, respectively. $\tilde{n}(C_L, sing.)$ is the dominant dimensionless frequency of an isolated cylinder at Re =46,000 (Mueller, 2012), and $22,000 \leq Re \leq 62,000$ (Knisely, 1990), calculated from C_L. $\tilde{n}(C_L, sing.)/\tilde{n}(C_L, clus.)$ and $\tilde{n}(u_x, sing.)/\tilde{n}(C_L, clus.)$ are the frequency ratio between the cluster and the single isolated cylinder, with the data in bracket are corresponding to (Knisely, 1990). The values of α in bracket are the closest incidence angles for the isolated cylinder in Knisely (1990), Mueller (2012) .

α	0°	11.25° (13°)	22.5° (20)°	33.75° (33)°	45°
$\tilde{n}(C_L, clus.)$	0.057	0.076	0.062	0.054	0.055
$\tilde{n}(u_x, clus.)$	0.062	0.076	0.062	0.053	0.050
$\tilde{n}(C_L, sing.)$ (Mueller, 2012)	0.117	0.143	0.11	0.108	0.106
$\tilde{n}(C_L, sing.)$ (Knisely, 1990)	0.13	0.155	0.14	0.130	0.125
$\tilde{n}(C_L, sing.)/\tilde{n}(C_L, clus.)$	2.1(2.3)	1.9(2.0)	1.8(2.3)	2.0(2.4)	1.9(2.3)
$\tilde{n}(u_x, sing.)/\tilde{n}(C_L, clus.)$	1.9(2.1)	1.9(2.0)	1.8(2.3)	2.0(2.5)	2.1(2.5)

4. Aerodynamic force characteristics of the cylinder cluster

Figure 10 shows the time series of the drag and lift coefficients of the four cylinders at $\alpha = 0°$. The drag coefficients of cylinders B2 and B3 fluctuate around a small negative average, while the average drag coefficients of cylinders B1 and B4 are positive, and close to that of a single isolated cylinder. On the other hand, the fluctuations of the drag and lift coefficients of cylinders B2 and B3 are more intense than those of B1 and B4, because the rear cylinder constrains the wake of the respective front cylinder. It is worth noting that, different from the single isolated square cylinder, the lift coefficient magnitudes of cylinders B1 and B4 have the average greater than unit. This is because of the channelling effect of the along-flow spacing between the cylinders.

A particular observation is that the drag and lift forces on the four cylinders are highly non-stationary, and different dynamical behaviour is observed in different time periods. During $t^* = 150 - 320$, the fluctuations are moderate, while during $t^* = 340 - 400$ and $t^* = 600 - 680$ they are more intense. This may imply the existence of different flow regimes which are very large in space and very slow in time, resulting from the complex interaction between the jet flow from the along-wind spacing and the vortex shedding from the exterior sides of the array of cylinders. The correlation coefficient of lift forces of B1 and B4 is -0.58, while that for B2 and B3 is -0.74 (Table 5), both confirming the strong impact of the channelling effect of the the along-wind spacing.

Figure 11 shows the time series of the aerodynamic force coefficients of the individual cylinders at $\alpha = 45°$. The forces on the B4 cylinder are very different from those on the other three cylinders, with a mean lift coefficient $\bar{C}_L \approx 0$ and very small drag fluctuations. One can speculate this is because the other three cylinders, in particular B1 and B3, prevent the B4's wake from developing to large oscillations. The drag and lift forces on cylinder B1 are highly correlated with those on cylinder B3 with correlation coefficients -0.92 and 0.53 (Table 5), respectively. This confirms Figure 9 that the cluster size vortex is shed from the cluster, as if it was an isolated, solid square cylinder with a width $2D$. Cylinder B2, which is placed deeper in the wake region than the other cylinders, experiences smaller drag and significantly larger fluctuating lift.

Figure 12a and Figure 12b show the time-averaged aerodynamic coefficients $\bar{C}_D$ and $\bar{C}_L$, respectively, of each cylinder at various incidence angles. For the drag coefficient $\bar{C}_D$ of an isolated square cylinder (e.g. Mueller, 2012), the maximum ($\bar{C}_D \approx 2$) occurs at $\alpha = 0°$ and 45°, while the minimum ($\bar{C}_D \approx 0.14$) occurs at $\alpha = 13°$. For the maximum magnitude of lift coefficient ($\bar{C}_L$ of an isolated square cylinder, the maximum ≈ 0.9) occurs at $\alpha = 13°$. At $\alpha = 0°$ and 45°, the mean lift coefficient $\bar{C}_L$ is approximately zero, as expected. Compared to the lift and drag coefficients of an isolated cylinder, the force coefficients of the individual cylinders of

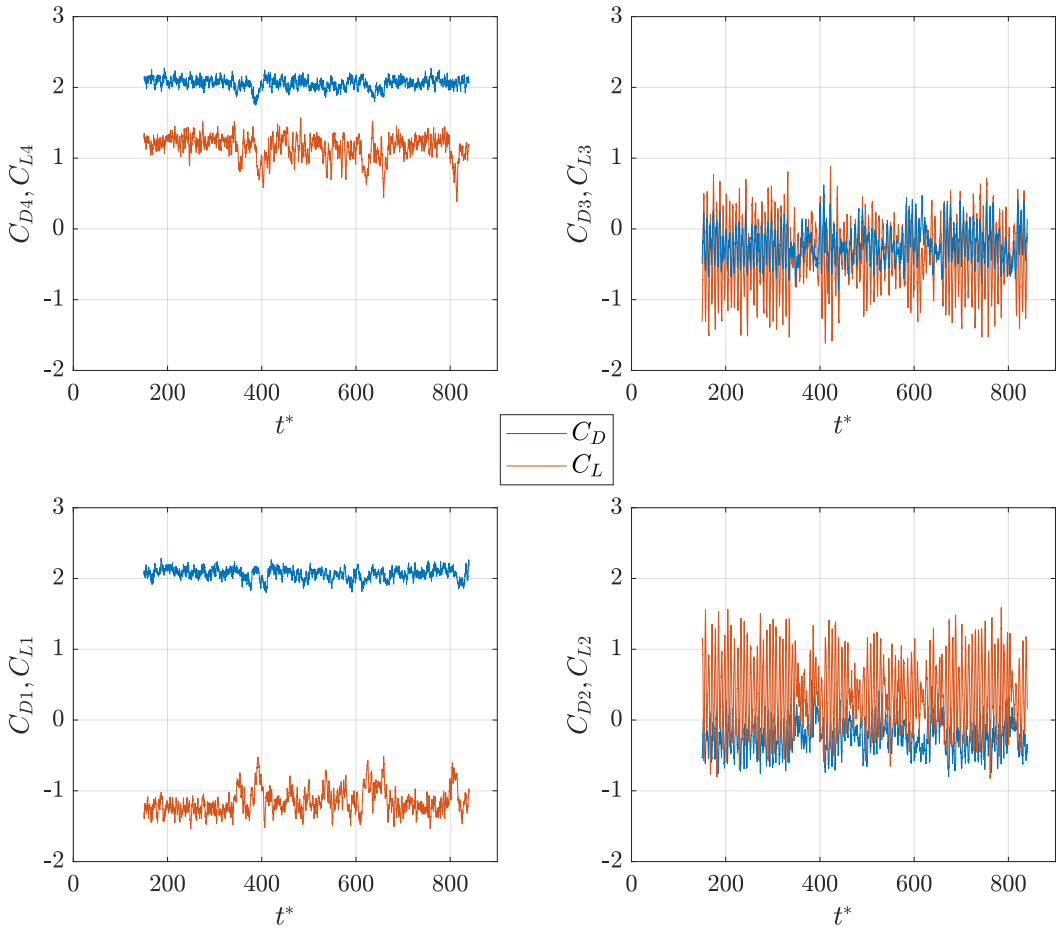

Figure 10: Time series of drag (C_{Di}) and lift (C_{Li}) coefficients of each cylinder at $\alpha = 0°$, where the subscript 'i' denotes the cylinder identification number (Figure 1); $t^* = tU_\infty/D$ is the non-dimensional time, where t is the dimensional flow time

the cluster show very complex interaction between them.

Figure 12c and Figure 12d show the time-averaged coefficients of the total drag (i.e. summation of the drag forces of the four cylinders) $\bar{C}_D^*$ and lift (i.e. summation of the lift forces of the four cylinders) $\bar{C}_L^*$, respectively. The $\bar{C}_D^*$ of the entire cluster at $\alpha = 45°$ is more than twice that at $\alpha = 0°$, whereas the drag of a single isolated cylinder at $\alpha = 45°$ is nearly the same as that at $\alpha = 0°$. This is because at $\alpha = 45°$ both the front area and the solidity (seen by the incoming flow) are substantially increased compared to at $\alpha = 0°$. Indeed, the $\bar{C}_D^*$ increases monotonically as the incidence angle increases. Figure 12d shows that the critical angle of incidence corresponding to the peak $\bar{C}_L^*$ occurs at $11.25° < \alpha < 22.5°$. This is somehow consistent with that of an isolated single cylinder, and is also associated with highest dominant frequency $\tilde{n} = 0.076$ for all the tested incidence angles (i.e. $0° \leq \alpha \leq 45°$). Again as expected, the total lift coefficient $\bar{C}_L^*$ is approximately 0 at $\alpha = 0$ and 45°.

Figure 13 shows the same as Figure 12 but for the root-mean-squared (r.m.s.) of the fluctuating drag ($\tilde{C}_D$) and lift $\tilde{C}_l$ coefficients. For individual cylinders, the $\tilde{C}_D$ and $\tilde{C}_L$ of cylinder B4

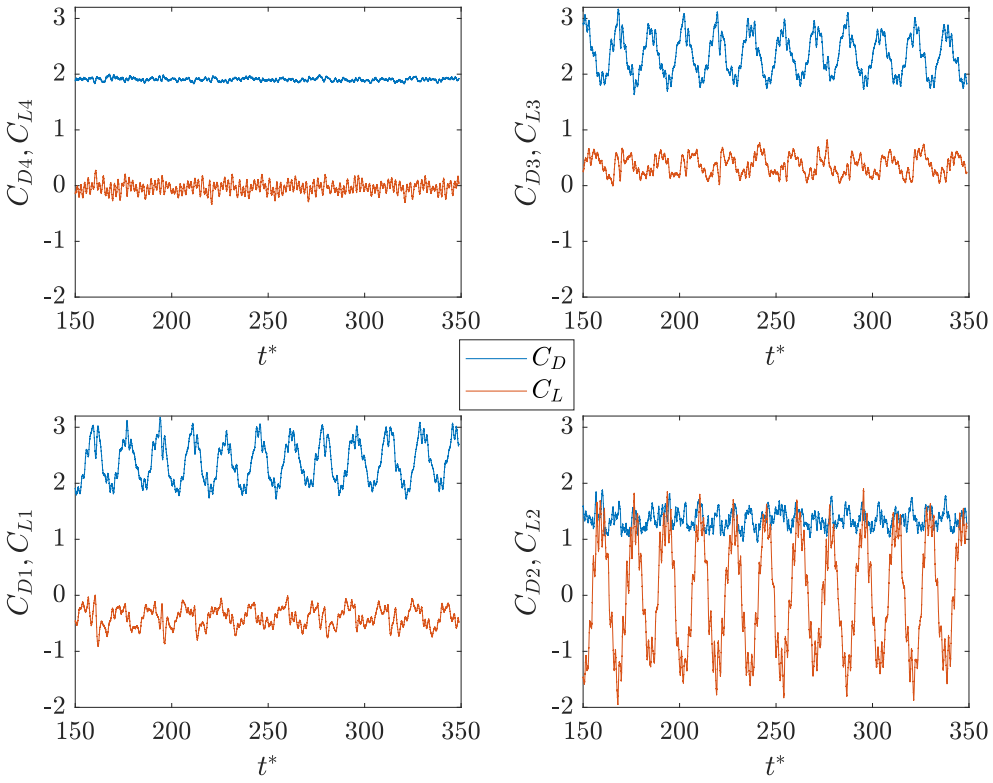

Figure 11: Same as in Fig. 10 but at $\alpha = 45°$

has small values and is almost unchanged with respect to wind directions. This is because it is always in the most upstream position in the cluster from which the shed vortices are constrained by the downstream cylinders resulting more steady aerodynamic forces of B4. Overall, Figure 13 shows very complex interactions between the individual cylinders.

In contrast to the extreme complexity of the $\tilde{C}_D$ of the individual cylinders shown in Figure 13, the tendency of the individual $\tilde{C}_L$ is simpler. As α increases, $\tilde{C}_L$ of cylinder B3 decreases to a small constant close to those of B1 and B4. Meanwhile, $\tilde{C}_L$ of cylinder B2 monotonically increases and has a significant maximum value at $\alpha = 45°$. At $\alpha = 45°$, cylinder B2 is fully in the wake and is open to the impact of the shed vortices, resulting in intensive fluctuating lift force much greater than that of the other cylinders (also see Figure 11). As a result, cylinder B2 provides a dominant contribution to the total lift fluctuations, leading to a monotonic increase of $\tilde{C}_L^*$ as shown in Figure 13d.

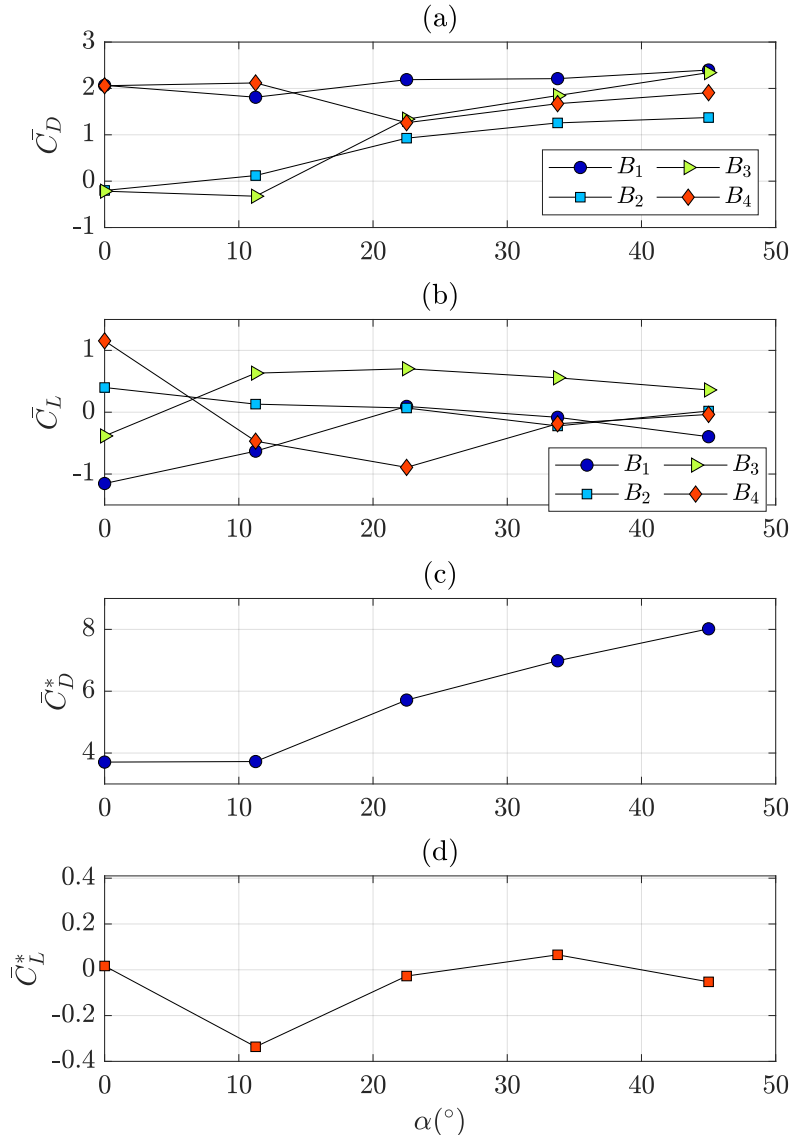

Figure 12: Time-averaged aerodynamic coefficients: (a) drag ($\bar{C}_D$); (b) lift ($\bar{C}_L$); (c) total drag ($\bar{C}_D^*$), and (d) total lift ($\bar{C}_L^*$)

In term of the dominant vortex shedding frequency, it is evident that the relevant data for the cluster can be scaled by $2D$ to be consistent with those for a single isolated cylinder, in particular in oblique incoming flows. Nevertheless, Figure 13c and d show that the trend against the incidence angle of the *r.m.s.* data (i.e. $\tilde{C}_D^*$, $\tilde{C}_L^*$) of total force fluctuations differs evidently from that for a singe isolated cylinder (e.g. Mueller, 2012). This suggests the complexity of the flow and aerodynamics of a cluster of cylinders.

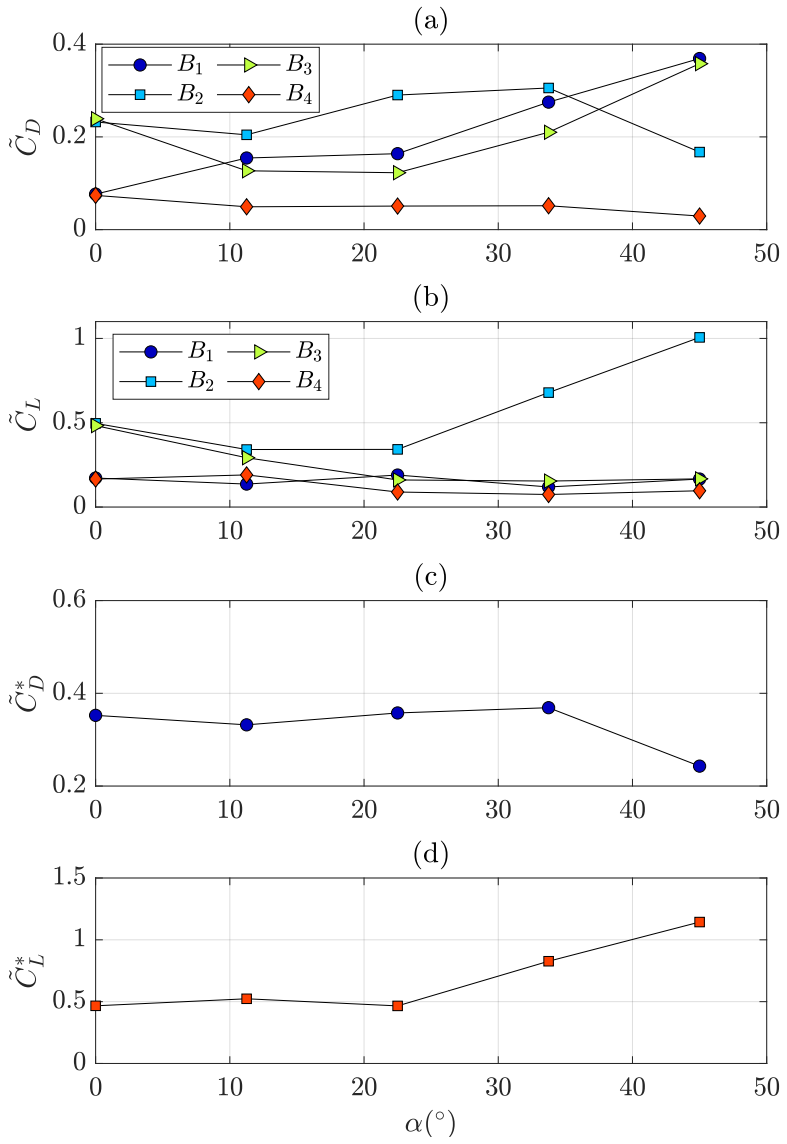

Figure 13: *r.m.s.* of aerodynamic coefficients: (a) drag ($\tilde{C}_D$); (b) lift ($\tilde{C}_L$); (c) total drag ($\tilde{C}_D^*$), and (d) total lift ($\tilde{C}_L^*$)

Given the complexity of the interaction between the cylinders, the correlation coefficients of the lift forces might be able to shed light on the interaction and the mechanism of the formation of the total forces. As $\alpha = 0°$ and $\alpha = 45°$ are respectively the minimum and maximum incidence angles, for which the correlation data are likely able to show a big map of correlation, Table 5 shows the correlation coefficients between the lift force of individual cylinders at these incidence angles.

At $\alpha = 0°$, the correlations of B1-B4 and B2-B3 are respectively -0.58 and -0.74. Meanwhile, the magnitude of other correlation coefficients are small, again suggesting strong channeling effect and the resulted pulsing jet effect due to the along-flow spacing between the cylinders.

At $\alpha = 45°$, the correlation data all show positive values, confirming the same tendency of the total lift $\tilde{C}_L^*$ and that of B2. It is worth noting that the correlation coefficient 0.53 of the pair B1-B3 suggests alternating cluster-size vortex shedding from B1 and B3 sides. The very small correlation coefficients of the pairs B4-B1 and B4-B3 suggests that the leading edgy vortices generated from B4 are not large enough to reattach on the entire cylinders B1 or B3, of which the lift forces are not correlated to that of B4 (Figure 8). The correlation coefficients of the pairs B1-B2 and B3-B2 are approximately 0.17. This suggests that the vortices generated from B1 or B3 are large enough to pass over or impact on cylinders B1 and B3. It is interesting that the correlation coefficient of the pair B4-B2 is 0.46. We speculate this is because the structures generated by cylinder B4 pass through the intersection of the cluster and impact on the cylinder B2 (Figure 8).

Table 5: Correlation coefficients between the lift force of individual cylinders at $\alpha = 0°$ and 45°. The bold numbers denote those at $\alpha = 45°$

$\alpha = 0°$ / $\alpha = 45°$	B1	B2	B3	B4
B1	1.00	0.12	0.10	-0.58
B2	**0.16**	1.00	-0.74	0.04
B3	**0.53**	**0.18**	1.00	0.16
B4	**0.01**	**0.46**	**0.02**	1.00

5. Conclusion

Rapid urban development with taller buildings and greater packing density requires a better understanding of the building aerodynamics and flow features in the wake region. A crucial attempt to achieve this goal has started with the investigation on arrays of prismatic cylinders, in particular to understand their interaction and the cluster effects. This is challenging because of the requirement of a very large domain to accommodate the wake development, and a Reynolds number greater than the critical one. The analysis of the data (such as the dominant vortex shedding frequency) is also challenging, as the commonly used Fourier transfer approach is not effective for such multiple-scale problems.

This paper addresses the challenges by carrying out large-eddy simulations with wavelet analysis for a 2x2 array of square cylinders at a Reynolds number equal to 22,000 at various flow incidence angles. The numerical settings, including the mesh resolution, were first validated extensively for a single isolated cylinder. Following the same settings as for the single isolated cylinder, simulations with further mesh sensitivity tests for a 2x2 array of square cylinders were carried out to ensure reliable and consistent data.

We found that the aerodynamic forces of the individual cylinders in the cluster substantially differed from each other, and from a single isolated cylinder. The aerodynamic forces were highly non-stationary suggesting different flow regimes. Engineering practice for estimating wind loading, even for clusters of buildings, is usually based on the aerodynamic coefficients (e.g. force, pressure) from a single isolated building. In addition, quasi-steady and stationary assumptions are often adopted. The current results suggest the importance of an improvement of the assessment of wind loading on densely packed tall buildings, and the impact of the wake flows.

The wavelet data of lift forces and fluctuating velocities in the wake show that the temporal dynamics of vortices shed from the cluster can be scaled by utilising a characteristic cluster size approximately equal to $2D$, despite that one might think of the cluster size being $3D$. This might be the product of the "permeability" of the cluster to the incoming wind. The shedding of large-scale vortices from the cluster is more intense at larger incidence angles, and relatively weaker at smaller ones. We speculate that this is because of the interaction between the flow developing within the cluster, e.g. the jet flow developing between the front cylinders at small incidence angles, and large-scale vortices shed from the cluster.

It is to be noted that the trend of the mean total aerodynamic forces of the cluster and in particular their *r.m.s.* data against the flow incidence angle differs evidently from that of an isolated single cylinder. This suggests that these aerodynamic force cannot simply be scaled by $2D$ for all incidence angles. Likely the width of the wake behind the cluster, and the deficit of

the wake velocity, cannot be scaled by $2D$, either. This is because of the non-linearity effect of the "permeability" of the cluster, and other more detailed mechanism, such as the pulsing jet within the cluster. Further studies performed for different separations between the buildings should be conducted to further elucidate the dependence of the characteristic length scale on the cluster parameters including the mean and *r.m.s*. data of the total aerodynamic forces.

6. Acknowledgement

The study presented in this paper is part of the UK Engineering and Physical Sciences Research Council (EPSRC)-funded project FUTURE (Grant EP/V010514/1). High performance computer systems at the University of Southampton, and the UK National Supercomputing system Archer2 via the UK Turbulence Consortium awards (Grants EP/D44073/1, EP/G06958/1, Project Code e01), were used for the massive compuational work. ZTX is grateful to Prof Alan Robins and Dr Marco Placidi for help discussions.

References

Agrawal, A., Djenidi, L., Antonia, R., 2006. Investigation of flow around a pair of side-by-side square cylinders using the lattice boltzmann method. Computers & fluids 35, 1093–1107.

Alam, M.M., Moriya, M., Takai, K., Sakamoto, H., 2002. Suppression of fluid forces acting on two square prisms in a tandem arrangement by passive control of flow. Journal of Fluids and Structures 16, 1073–1092.

Alam, M.M., Zhou, Y., Wang, X., 2011. The wake of two side-by-side square cylinders. Journal of Fluid Mechanics 669, 432–471.

Bearman, P., Obasaju, E., 1982a. An experimental study of pressure fluctuations on fixed and oscillating square-section cylinders. Journal of Fluid Mechanics 119, 297–321.

Bearman, P.W., Obasaju, E.D., 1982b. An experimental study of pressure fluctuations on fixed and oscillating square-section cylinders. Journal of Fluid Mechanics 119, 297–321. doi:10.1017/S0022112082001360.

Burattini, P., Agrawal, A., 2013. Wake interaction between two side-by-side square cylinders in channel flow. Computers & Fluids 77, 134–142.

Cao, Y., Tamura, T., 2016. Large-eddy simulations of flow past a square cylinder using structured and unstructured grids. Computers & Fluids 137, 36–54.

Chen, Y., Djidjeli, K., Xie, Z.T., 2020. Large eddy simulation of flow past stationary and oscillating square cylinders. Journal of Fluids and Structures 97, 103107.

Du, X., Chen, R., Dong, H., Ma, W., Xu, H., Zhao, Y., 2021. Aerodynamic characteristics of two closely spaced square cylinders in different arrangements. Journal of Wind Engineering and Industrial Aerodynamics 208, 104462.

Han, Z., Zhou, D., Tu, J., Fang, C., He, T., 2014. Flow over two side-by-side square cylinders by cbs finite element scheme of spalart–allmaras model. Ocean Engineering 87, 40–49.

Horiguchi, M., Hayashi, T., Adachi, A., Onogi, S., 2012. Large-scale turbulence structures and their contributions to the momentum flux and turbulence in the near-neutral atmospheric boundary layer observed from a 213-m tall meteorological tower. Boundary-layer meteorology 144, 179–198.

Inagaki, M., Kondoh, T., Nagano, Y., 2005. A mixed-time-scale sgs model with fixed model-parameters for practical les. Journal of Fluids Engineering 127, 1–13.

Kahil, Y., Benhamadouche, S., Berrouk, A.S., Afgan, I., 2019. Simulation of subcritical-reynolds-number flow around four cylinders in square arrangement configuration using les. European Journal of Mechanics-B/Fluids 74, 111–122.

Knisely, C.W., 1990. Strouhal numbers of rectangular cylinders at incidence: a review and new data. Journal of fluids and structures 4, 371–393.

Mahrt, L., 1991. Eddy asymmetry in the sheared heated boundary layer. Journal of Atmospheric Sciences 48, 472–492.

Mueller, A., 2012. Large eddy simulation of cross-flow around a square rod at incidence with application to tonal noise prediction. PhD's thesis, University of twente, Holland.

Nguyen, C.H., Macdonald, J.H.G., Cammelli, S., 2020. Non-across-wind galloping of a square-section cylinder. Meccanica 55, 1333–1345. doi:10.1007/s11012-020-01166-6.

Nguyen, C.H., Nguyen, D.T., Owen, J.S., Hargreaves, D.M., 2022. Wind tunnel measurements of the aerodynamic characteristics of a 3: 2 rectangular cylinder including non-gaussian and non-stationary features. Journal of Wind Engineering and Industrial Aerodynamics 220, 104826.

Norberg, C., 1993. Flow around rectangular cylinders: Pressure forces and wake frequencies. Journal of Wind Engineering and Industrial Aerodynamics 49, 187–196. doi:10.1016/0167-6105(93)90014-F.

Olhede, S., Walden, A., 2002. Generalized morse wavelets. IEEE Transactions on Signal Processing 50, 2661–2670. doi:10.1109/TSP.2002.804066.

Perrier, V., Philipovitch, T., Basdevant, C., 1995. Wavelet spectra compared to fourier spectra. Journal of Mathematical Physics 36, 1506–1519. doi:10.1063/1.531340.

Sau, A., Hsu, T.W., Ou, S.H., 2007. Three-dimensional evolution of vortical structures and associated flow bifurcations in the wake of two side-by-side square cylinders. Physics of Fluids 19, 084105.

Tamura, T., Miyagi, T., 1999. The effect of turbulence on aerodynamic forces on a square cylinder with various corner shapes. Journal of Wind Engineering and Industrial Aerodynamics 83, 135–145. doi:https://doi.org/10.1016/S0167-6105(99)00067-7.

Trias, F., Gorobets, A., Oliva, A., 2015. Turbulent flow around a square cylinder at Reynolds number 22,000: A DNS study. Computers & Fluids 123, 87–98.

Zhang, J., Chen, H., Zhou, B., Wang, X., 2019. Flow around an array of four equispaced square cylinders. Applied Ocean Research 89, 237–250.